

Sager, W., Hoernle, K., Höfig, T.W., Blum, P., and the Expedition 391 Scientists *Proceedings of the International Ocean Discovery Program* Volume 391 publications.iodp.org







# Expedition 397T summary<sup>1</sup>

#### Contents

- 1 Abstract
- 2 Introduction
- 4 Background
- **6** Scientific objectives
- 7 Site summaries
- **18** Preliminary scientific assessment
- 20 Connections to the 2050 Science Framework
- 20 References

#### Kevwords

International Ocean Discovery Program, IODP, JOIDES Resolution, Expedition 391, Expedition 397T, Walvis Ridge Hotspot, Site U1584, Site U1585, Earth Connections, Tristan-Gough-Walvis Hotspot, true polar wander, isotopic zonation, large low shear-wave velocity province, LLSVP

#### **Core descriptions**

**Supplementary material** 

#### References (RIS)

MS 391-109 Published 11 October 2023

Funded by NSF OCE1326927

W. Sager, P. Blum, C.A. Carvallo, D. Heaton, W.R. Nelson, M. Tshiningayamwe, M. Widdowson, and the Expedition 391 Scientists<sup>2</sup>

<sup>1</sup> Sager, W., Blum, P., Carvallo, C.A., Heaton, D., Nelson, W.R., Tshiningayamwe, M., Widdowson, M., and the Expedition 391 Scientists, 2023. Expedition 397T summary. In Sager, W., Hoernle, K., Höfig, T.W., Blum, P., and the Expedition 391 Scientists, Walvis Ridge Hotspot. Proceedings of the International Ocean Discovery Program, 391: College Station, TX (International Ocean Discovery Program). https://doi.org/10.14379/iodp.proc.391.109.2023

# **Abstract**

International Ocean Discovery Program Expedition 397T sought to address the shortage of drilling time caused by COVID-19 mitigation during Expedition 391 (Walvis Ridge Hotspot) by drilling at two sites omitted from the earlier cruise. A week of coring time was added to a transit of JOIDES Resolution from Cape Town to Lisbon, which would cross Walvis Ridge on its way north. These two sites were located on two of the three seamount trails that emerge from the split in Walvis Ridge morphology into several seamount chains at 2°E. Site U1584 (proposed Site GT-6A) sampled the Gough track on the southeast side of the hotspot track, and Site U1585 (proposed Site TT-4A) sampled the Tristan track on the northwest side. Together with Site U1578, drilled on the Center track during Expedition 391, they form a transect across the northern Walvis Ridge Guyot Province. The goal was to core seamount basalts and associated volcanic material for geochemical and isotopic, geochronologic, paleomagnetic, and volcanological study. Scientifically, one emphasis was to better understand the split in isotopic signatures that occurs at the morphologic split. Geochronology would add to the established age progression but also give another dimension to understanding Walvis Ridge seamount formation by giving multiple ages at the same sites. The paleomagnetic study seeks to establish paleolatitudes for Walvis Ridge sites for comparison with those published from hotspot seamount chains in the Pacific, in particular to test whether a component of true polar wander affects hotspot paleolatitude.

Hole U1584A cored a 66.4 m thick sedimentary and volcaniclastic section with two lithostratigraphic units. Unit I is a 23 m thick sequence of bioturbated clay and nannofossil chalk with increasing volcaniclastic content downhole. Unit II is a >43 m thick sequence of lapillistone with basalt fragments. Because the seismic section crossing the site shows no evidence as to the depth of the volcaniclastic cover, coring was terminated early. Because there were no other shallow sites nearby with different characteristics on existing seismic lines, the unused operations time from Site U1584 was shifted to the next site.

The seismic reflector interpreted as the top of igneous rock at Site U1585 once again resulted from volcaniclastic deposits. Hole U1585A coring began at 144.1 mbsf and penetrated a 273.5 m thick sedimentary and volcaniclastic section atop a 81.2 m thick series of massive basalt flows. The hole was terminated at 498.8 mbsf because allotted operational time expired. The sedimentary section contains four main lithostratigraphic units. Unit I (144.1–157.02 mbsf) is a bioturbated nannofossil chalk with foraminifera, similar to the shallowest sediments recovered at Site U1584. Unit II (157.02–249.20 mbsf), which is divided into two subunits, is a 92.2 m thick succession of massive and bedded pumice and scoria lapillistone with increased reworking, clast alteration, and tuffaceous chalk intercalations downhole. Unit III (249.20–397.76 mbsf) is 148.6 m thick and consists of a complex succession of pink to greenish gray tuffaceous chalk containing multiple thin, graded ash turbidites and tuffaceous ash layers; intercalated tuffaceous chalk slumps; and several thick coarse lapilli and block-dominated volcaniclastic layers. Befitting its complexity, this unit is

<sup>&</sup>lt;sup>2</sup>Expedition 397T Scientists' affiliations.

divided into eight subunits (IIIA–IIIH). Three of these subunits (IIIA, IIID, and IIIG) are mainly basalt breccias. Unit IV (397.76–417.60 mbsf) is a volcanic breccia, 19.8 m thick, containing mostly juvenile volcaniclasts. The igneous section, Unit V (417.60–498.80 mbsf) is composed of a small number of massive basaltic lava flows. It is divided into three igneous lithologic units, with Unit 2 represented by a single 3 cm piece of quenched basalt with olivine phenocrysts in a microcrystalline groundmass. This piece may represent a poorly recovered set of pillow lavas. Unit 1 is sparsely to highly olivine-clinopyroxene ± plagioclase phyric massive basalt and is divided into Subunits 1a and 1b based on textural and mineralogical differences, which suggests that they are two different flows. Unit 3 also consists of two massive lava flows with no clear boundary features. Subunit 3a is a 10.3 m thick highly clinopyroxene-plagioclase phyric massive basalt flow with a fine-grained groundmass. Subunit 3b is a featureless massive basalt flow that is moderately to highly clinopyroxene-olivine-plagioclase phyric and >43.7 m thick. Alteration of the lava flows is patchy and moderate to low in grade, with two stages, one at a higher temperature and one at a low temperature, both focused around fractures.

The Site U1585 chronological succession from basalt flows to pelagic sediment indicates volcanic construction and subsidence. Lava eruptions were followed by inundation and shallow-water volcaniclastic sediment deposition, which deepened over time to deepwater conditions. Although the massive flows were probably erupted in a short time and have little variability, volcaniclasts in the sediments may provide geochemical and geochronologic data from a range of time and sources. Chemical analyses indicate that Site U1585 basalt samples are mostly alkalic basalt, with a few trachybasalt flow and clast samples and one basaltic trachyandesite clast. Ti/V values lie mostly within the oceanic island basalt (OIB) field but overlap the mid-ocean-ridge basalt (MORB) field. Only a handful of clasts from Site U1584 were analyzed, but geochemical data are similar. Paleomagnetic data from Site U1585 indicate that the sediments and basalt units are strongly magnetic and mostly give coherent inclination data, which indicates that the basaltic section and ~133 m of overlying volcaniclastic sediment is reversely polarized and that this reversal is preserved in a core. Above this, the rest of the sediment section records two normal and two reversed zones. Although there are not enough basalt flows to give a reliable paleolatitude, it may be possible to attain such a result from the sediments.

# 1. Introduction

International Ocean Discovery Program (IODP) Expedition 397T sought to address the omission of two drill sites during Expedition 391 (Walvis Ridge Hotspot) caused by loss of time due to COVID-19 mitigation. The R/V *JOIDES Resolution* would necessarily pass over Walvis Ridge on its transit north from Cape Town to Lisbon to begin a campaign of northern hemisphere drilling. Making the most of the opportunity, 7 days of operations time were added to the transit for coring at Walvis Ridge. The drilling time was limited to that amount by the length of the transit (Figure F1) and maintenance of the ship's schedule. Despite the limited operations time, it was decided to attempt coring at two sites on what was originally planned as a three-site transect for Expedition 391. The transect crosses the two, possibly three, seamount chains in the Walvis Ridge Guyot Province at a location slightly younger than the morphologic split of the chain from one to three chains (Figure F2). The three possible chains have the provisional names Tristan track, Center track, and Gough track, with the first and last names indicating that the western and eastern chains lead to the volcanically active islands of the Tristan da Cunha group and Gough. A hole was drilled at Site U1578 into ~302 m of a volcanic sequence on a Center track seamount during Expedition 391 (Figure F2). The aim of Expedition 397T was to sample the two outboard seamount chains at proposed Sites GT-6A (Gough track) and TT-3A (Tristan track).

It was clear that this goal was aspirational because the combined estimated operations time for the two sites, from Expedition 391 planning, was 9.3 days, but only 7 operational days were allotted to Expedition 397T. Recognizing this time squeeze, planning sought to reduce operations that were not related to coring igneous rock, the main goal of the project. The shallowest sites were chosen, Site GT-6A on the upper flank of the Gough track seamount and Site TT-3A on the top of the Tristan track seamount. Shallower sites require less core retrieval wireline time. Site GT-6A was a new site proposed to take advantage of thinner sediment near the edge of the flank sediment pile.

Drilling without coring through most of the sediment package was approved for both sites because these sediments would be similar to those cored at Site U1578. To further save time, the mudline was established for both sites by lowering the bottom-hole assembly (BHA) to the estimated seafloor depth and coring until sediment was encountered. This required less time than sending a camera down the drill string to observe the sea bottom. Even with attempts to minimize drill time, Expedition 397T required a healthy dose of geologic luck. Site U1578 was just right, with a long series of lava flows that cored easily underlying a short sediment section. The basalt units contained abundant glass, geochemical variations, and minerals sought by geochemists for study.

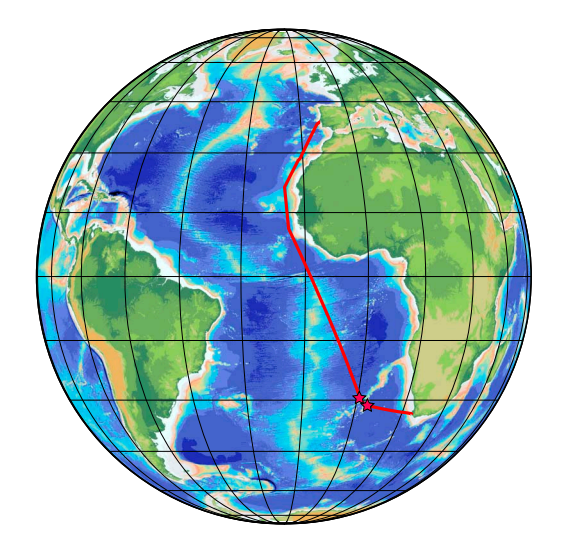


**Figure F1.** Expedition 397T transit path (red line). Stars show locations of Sites U1584 and U1585. Topography is from the GMRT synthesis (Ryan et al., 2009).

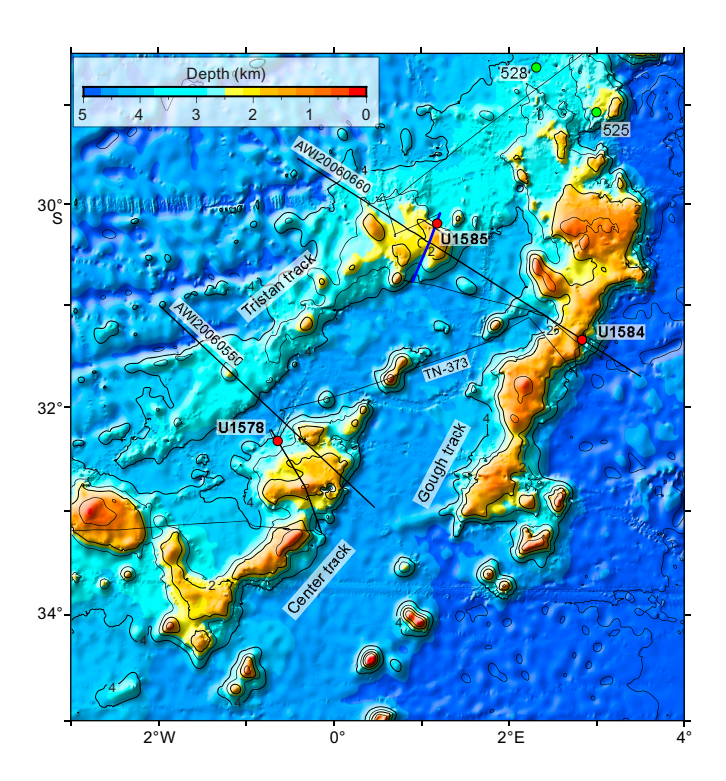


**Figure F2.** Bathymetry map of the northern Guyot Province, showing the Tristan, Gough, and Center track edifices, as well as drill sites for Expeditions 391 and 397T. Heavy blue line = Seismic Line TT-01. Red dots = Expedition 391 and 397T site locations. Green dots = the southern two sites (525 and 528) that recovered basalt in the DSDP Leg 74 transect (Moore et al., 1984). Plotted bathymetry is the SRTM15+ predicted bathymetry data set (Tozer et al., 2019). Contour interval is 1 km.

Table T1. Hole summary, Expedition 397T. DSF = drilling depth below seafloor. Download table in CSV format.

Hole	Latitude	Longitude	Water depth (m)	Penetration DSF (m)		Recovered length (m)	Recovery (%)	Drilled interval (m)	Drilled interval (N)	Total cores (N)	RCB cores (N)	Date started UTC (h)	Date finished UTC (h)	Time on hole (days)
U1584A	31°20.322′S	2°50.221′E	2305	208.2	75.2	23.68	31.49	133	1	8	8	15 Sep 2022 0745	17 Sep 2022 0500	1.89
U1585A	30°10.016′S	1°10.649′E	3457	498.8	355.6	217.73	61.23	143.2	1	38	38	17 Sep 2022 1545	23 Sep 2022 1500	5.97
		Expediti	on totals:	707	430.8	241.41		276.2	2	46	46			

However, the Expedition 397T sites were not as cooperative. They rather served as a reminder that seamount geology is complex and poorly understood and drilling options are usually constrained by limited academic site survey data. Drilling at Site U1584 (proposed Site GT-6A) plunged into volcaniclastics with no seismic evidence of a bottom. Because there were no other sites that had a different character, the decision was made to terminate coring early after only 66.4 m of coring (Table T1). The unused time was shifted to the next site, U1585. Because a guyot summit may accumulate volcaniclastics from shallow-water eruptions, a decision was made to drill proposed Site TT-4A on the lower flank of the same volcano as proposed Site TT-3A. The seismic section across the site has a similar appearance to that of Site U1578. The extra wireline time for the deeper site would be made up with time saved from Site U1584. Drilling at Site U1585 (proposed Site TT-4A) also plunged into a thick volcaniclastic section, and core after core of volcaniclastic sediments were recovered. Finally, at 417.6 mbsf, lava flows were encountered and cored to the bottom of the hole (498.8 mbsf) until time expired (Table T1).

# 2. Background

The scientific background for Walvis Ridge hotspot drilling is given at length in the Expedition 391 summary chapter (Sager et al., 2023), so only an outline is given here. Walvis Ridge is a long, quasilinear ridge and seamount chain that stretches from the African margin to the active volcanoes of Tristan da Cunha and Gough Island (Figure F3). It is thought that Walvis Ridge volcanism began around 132 Ma with eruption of the Etendeka flood basalt. Because of the apparent age progression, Walvis Ridge was an early candidate for a hotspot ridge caused by plate motion over a stationary mantle plume (Morgan, 1971, 1981). It is one of only a handful considered to be a "primary" plume originating in the deep mantle (Courtillot et al., 2003). Early radiometric dates and reconstructions indicated that Walvis Ridge began with the hotspot at the Mid-Atlantic Ridge, where it formed the larger Walvis Ridge edifice along with Rio Grande Rise, a conjugate large igneous province (LIP) on the South American plate (O'Connor and Duncan, 1990). Around 70 Ma, the hotspot and Mid-Atlantic Ridge separated, with the hotspot ending up beneath the African plate, where it formed the seamounts and ridges of the Walvis Ridge Guyot Province (O'Connor and Duncan, 1990; O'Connor and Jokat, 2015a, 2015b). Subsequent geochronology studies have refined the age data to produce a tight linear trend of volcano age progression along the Tristan-Gough-Walvis Ridge hotspot track (Walvis Ridge and the Guyot Province) (Figure F4) (Rohde et al., 2013; O'Connor and Jokat, 2015a; Homrighausen et al., 2019, 2020).

Although the Walvis Ridge and its extension to the Guyot Province is the most prominent Atlantic hotspot track, it nevertheless contains complications to the simple plume model. Starting at the Deep Sea Drilling Project (DSDP) Leg 74 transect, which is slightly north of the morphologic split between Walvis Ridge and the Guyot Province (Figures F2, F3), there are two distinct trails of Pbisotope signatures, one characterizing the seamount track that leads to Tristan da Cunha and the other characteristic of the seamounts leading to Gough Island (Rohde et al., 2013; Hoernle et al., 2015). The ridge formed prior to the morphologic split (farther northeast) has the Gough Island isotopic signature (Hoernle et al., 2015). Thus, Walvis Ridge displays the oddity not only that it splits from a single ridge to two or more but that the isotopic signature splits occur at roughly the same time. Although isotopic zonation is observed in other hotspot seamount chains, the ~70 Ma split makes the Walvis Ridge Guyot Province one of the longest documented examples of such zonation (Hoernle et al., 2015). An explanation for the zonation is the tapping of two different zones of source material at the edge of the Atlantic large low shear-wave velocity province

(LLSVP) at the core mantle boundary (Hoernle et al., 2015; Homrighausen et al., 2018). Unpublished isotopic data suggest that the Center track may constitute an additional isotopic zonation (Class et al., 2015) or it may be a result of mixing of Tristan and Gough signatures. If the former, it may require rethinking of the zonation model.

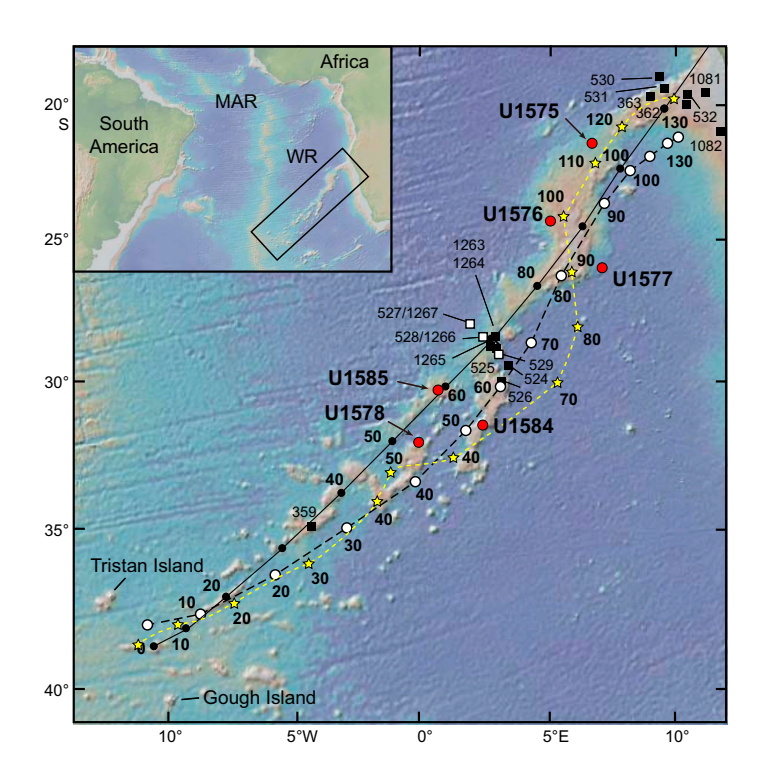


**Figure F3.** Walvis Ridge bathymetry (GMRT synthesis; Ryan et al., 2009), hotspot age models, previous drill sites, and proposed drill sites. Solid line = central plume track of the O'Connor and Le Roex (1992) hotspot model, with dots every 10 Ma. Dashed line = Torsvik et al. (2008) fixed hotspot model, with circles every 10 Ma. Yellow stars and dashed line = moving hotspot model of Doubrovine et al. (2012). Small bold numbers give ages in Ma. Squares = DSDP and ODP holes drilled along Walvis Ridge. Red dots = drill sites for Expeditions 391 and 397T. Inset shows location of Walvis Ridge (WR) in the South Atlantic. MAR = Mid-Atlantic Ridge.

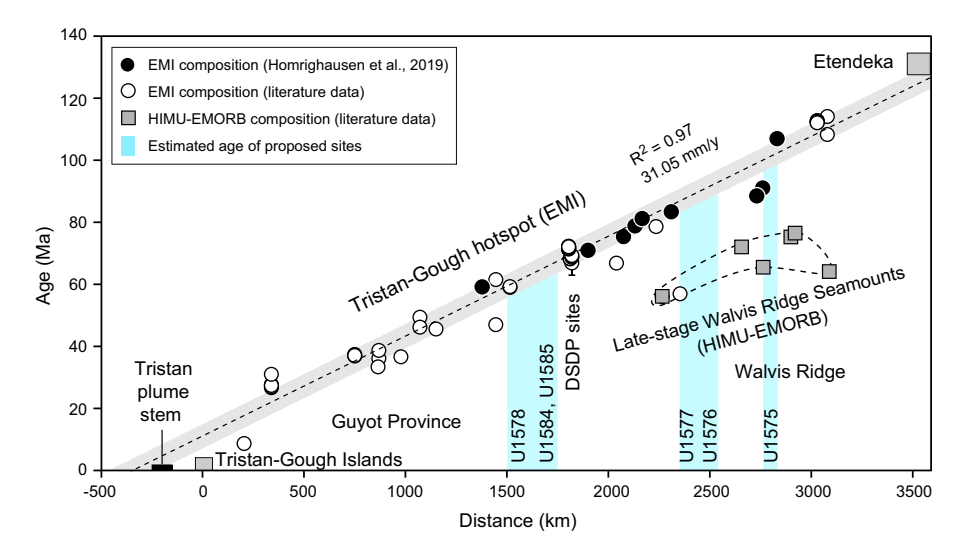


**Figure F4.** Walvis Ridge age progression from radiometrically dated igneous rocks. Samples with enriched mantle one (EMI) composition follow a tight linear trend. Exceptions are samples with high  $\mu$  (HIMU)-type composition that yield ages  $\sim$ 30–40 My younger than the underlying basement with an EMI-type geochemical composition. Vertical blue bands = Expedition 391 and 397T sites, denoting estimated ages (see Homrighausen et al., 2019, for sources of age data).

Another anomaly is the occurrence in Walvis Ridge of another linear age trend with a different isotopic signature and a gap of ~30–40 Ma after the older age trend (Homrighausen et al., 2019, 2020). This late-stage volcanism is attributed to another source of buoyant plume material rising from the top of the LLSVP (Homrighausen et al., 2019, 2020). Valdivia Bank represents a tectonic anomaly. It is an oceanic plateau incorporated into Walvis Ridge and represents two sharp bends in the chain because its trend is at high angle to the Walvis Ridge trend. Recent reconstruction of Walvis Ridge and Rio Grande Rise suggests that Valdivia Bank and Rio Grande Rise formed at the Mid-Atlantic Ridge while it was undergoing a reorganization during the Late Cretaceous that formed a microplate (Sager et al., 2021). This tectonic event may have disturbed the age progression because the model implies that Valdivia Bank formed from east—west spreading rather than a north—south hotspot age progression typical of most hotspot models (e.g., Doubrovine et al., 2012).

Walvis Ridge has important implications for another geodynamic problem, the import of hotspots as plate motion indicators. Hotspots were initially viewed as being fixed markers in the mantle, formed by deep plumes rising to the surface, which would allow plate motions to be determined from hotspot seamount trends and age progressions (e.g., Morgan, 1971, 1981; Müller et al., 1993). As the longest and most continuous hotspot track in the Atlantic Ocean, Walvis Ridge has been a foundation for hotspot models of African plate motion (Duncan, 1981). Nevertheless, hotspot models for Walvis Ridge have trouble fitting its complex morphology (O'Connor and Le Roex, 1992; Torsvik et al., 2008; Doubrovine et al., 2012). Additional age data and studies of Walvis Ridge tectonic anomalies are required to sort out these problems. Walvis Ridge also has important potential to understand whether or how hotspots define a mantle reference frame and the behavior of that reference frame.

DSDP and Ocean Drilling Program (ODP) studies of the paleomagnetism of drill cores from the Hawaiian-Emperor seamount chain demonstrated that from about 80-50 Ma, its hotspot moved southward by ~10°-15° (Kono, 1980; Tarduno and Cottrell, 1997; Tarduno et al., 2003). An early explanation for this shift was that the Earth's spin axis shifted away from the Pacific Ocean, a process termed "true polar wander" (TPW) (Gordon and Cape, 1981; Gordon, 1987). TPW has been documented on other planets and moons as well as at other times in Earth's past (e.g., Gold, 1955; Goldreich and Toomre, 1969; Tsai and Stevenson, 2007; Torsvik et al., 2010; Creveling et al., 2012). But has it happened since the Late Cretaceous? Integrated Ocean Drilling Program Expedition 330 did a similar study of another Pacific hotspot, the Louisville Ridge, documenting less paleolatitude change (Koppers et al., 2012). Other scientists questioned the fixity of hotspots for other reasons, and this led to the view that most hotspot paleolatitude changes have been caused by hotspot motion attributed to mantle flow, rather than by TPW (e.g., Tarduno et al., 2009). Nevertheless, recent research suggests that TPW has occurred since the Late Cretaceous (Woodworth and Gordon, 2018; Zheng et al., 2018; Gordon et al., 2019), so the implication is that TPW is combined with hotspot motion during this time. Thus, additional studies of changes in hotspot paleolatitudes are needed. This was recognized by the 2007 Hotspot Geodynamics Detailed Planning Group, which recommended coring Walvis Ridge seamounts to determine paleolatitude for comparison with Pacific hotspots (Duncan et al., 2007). Moreover, paleolatitude inferred for Walvis Ridge from combined continental paleomagnetic poles implies that the paleolatitude during early Cenozoic was 4°-6° farther south than at present, an anomaly that is not explained by hotspot drift models but may be an indication of TPW that caused Pacific hotspots to move south while Atlantic hotspots moved north.

# 3. Scientific objectives

The main goal of Expedition 397T coring was to recover basalts and associated volcanic material for geochemical, geochronological, paleomagnetic, and volcanological study. Coring at two sites in the northern Walvis Ridge Guyot Province aimed to complete the three-site transect across the three seamount chains originally planned for Expedition 391 but left unfinished because of cuts in operations time due to a COVID-19 outbreak on board. Specific objectives were as follows; most rely upon recovering fresh basalt samples:

- Determine isotopic signatures of basalt flows to determine whether the Center track (Site U1578) represents a different composition or a mixture of Tristan and Gough lavas. Data will be used to understand the isotopic zonation.
- Analyze major and trace element and isotope compositions to determine the mantle sources of the magmas and depth and degree of melting. Such information will be used to better understand the generation of seamounts from the melting of a mantle plume.
- Create major and trace element chemistry and isotope stratigraphy for successions of lava flows to learn about changes in the source through the evolution of the seamount.
- Determine multiple high-precision radiometric dates from lava successions to determine the temporal evolution of a hotspot seamount. Most seamounts have only one age because the sample comes from a dredge.
- Create a geologic record of seamount volcanism to better understand the formation and evolution of Walvis Ridge guyots.
- Collect samples from multiple basalt flows to measure for paleomagnetic inclination, which will be used to determine hotspot paleolatitude. Walvis Ridge paleolatitude will be compared with coeval Pacific hotspot paleolatitudes to see if there is a coherent shift (TPW).
- Collect sediment samples to measure for paleomagnetic inclination to complement studies of basalt inclination.

# 4. Site summaries

#### 4.1. Site U1584

#### 4.1.1. Background and objectives

Site U1584 was planned to sample a Gough track ridge to provide basalt samples that would anchor the Gough end of a geochemical transect across the Walvis Ridge Guyot Province (Figure F2). The location was chosen to be slightly younger than the morphologic split in Walvis Ridge, which roughly coincides with the development of different geochemical signatures for the different guyot chains. The major objectives were to core basalt lava flows for major and trace element and isotope geochemistry, obtain fresh basalt samples for geochronology, and recover multiple lava units for paleomagnetic inclination studies. Unfortunately, coring quickly encountered indurated volcaniclastic deposits. Seismic data does not indicate a limit to such deposits, and because there were no alternative sites (or enough time to address them), the science team elected to quit Site U1584 and save the unused operations time for the next site.

#### 4.1.2. Operations

Expedition 397T began on 10 September 2022, 0800 h (UTC + 2), with the ship tied up at Duncan Dock E, Cape Town, South Africa. All oncoming Expedition 397T personnel, including 22 *JOIDES Resolution* Science Operator (JRSO) staff and 8 scientists, moved onto the ship following a 4 day hotel quarantine. The quarantine included a PCR and an antigen test according to the COVID-19 mitigation protocol. All personnel tested negative. Once onboard, all shipboard personnel received another COVID-19 PCR test, and all were negative. Port call activities continued, including the loading of 500 mt of fuel and fresh food. COVID-19 mitigation protocols continued to be followed throughout port operations. One more JRSO staff member came on board before the pilot boarded and the ship departed Cape Town on 12 September at 1018 h.

At 0200 h on 15 September, the ship's clock was set back 1 h to UTC + 1. We completed the 810 nmi voyage from Cape Town and arrived at Site U1584 (proposed Site GT-06A) at 0830 h. The thrusters were deployed, and a drill string with a rotary core barrel (RCB) BHA and a C-4 coring bit was assembled. At 1630 h, the top drive was engaged and a pipe-cleaning device (pig) was deployed to clear potential rust and other obstructions from the drill pipe. We estimated the seafloor at 2313 meters below rig floor (mbrf) based on the corrected precision depth recorder (PDR) signal. At 1800 h, the first core barrel was dropped from 2310 mbrf, and the liner returned empty. The driller had observed a tag at 2315.9 mbrf while lowering the core barrel. For the second attempt, the barrel was dropped from 2315.9 mbrf. The liner returned empty again except for sediment residue smeared all along its length, indicating that the barrel had penetrated the formation

but couldn't hold the sediment. At 2005 h, we declared the seafloor depth at 2315.9 mbrf and deployed the core barrel. The barrel with the center bit had to be deployed twice because no indication of landing was detected the first time. We started to drill down without coring, reaching the target at 141.8 meters below seafloor (mbsf) at 0515 h on 16 September. The wash barrel was retrieved, and the RCB core barrel was deployed. RCB coring proceeded from Core 397T-U1584A-3R through Core 9R (141.8–208.2 mbsf), with core recovery ranging 0%–95% (average = 36%). Hole U1584A was swept with 30 bbl (4769.6 L) of sepiolite mud after Cores 5R (170 mbsf) and 9R (208.2 mbsf).

At 2215 h on 16 September, we decided to terminate operations at Site U1584 because the seismic basement reflector turned out to be the top of a potentially thick succession of volcaniclastic sediments rather than the desired basaltic lava flows. We retrieved the drill string from Hole U1584A, and the bit cleared the rig floor at 0605 h on 17 September. The rig floor was secured, the thrusters were raised, and we departed Site U1584 at 0700 h. The total time spent on Site U1584 was 45.4 h, or 1.89 days.

COVID-19 mitigation protocols continued to be followed with mask wearing, social distancing and antigen testing of all personnel. Four individuals tested positive after boarding the ship on 11, 13 (2 people), and 15 September. They were isolated until antigen tests on two successive days, starting on Day 5, were negative.

#### 4.1.3. Lithostratigraphy

A >65 m thick succession of sediments was drilled at Site U1584 (Figure **F5**). It comprises two main lithostratigraphic units, an upper chalky pelagic sediment passing into highly bioturbated

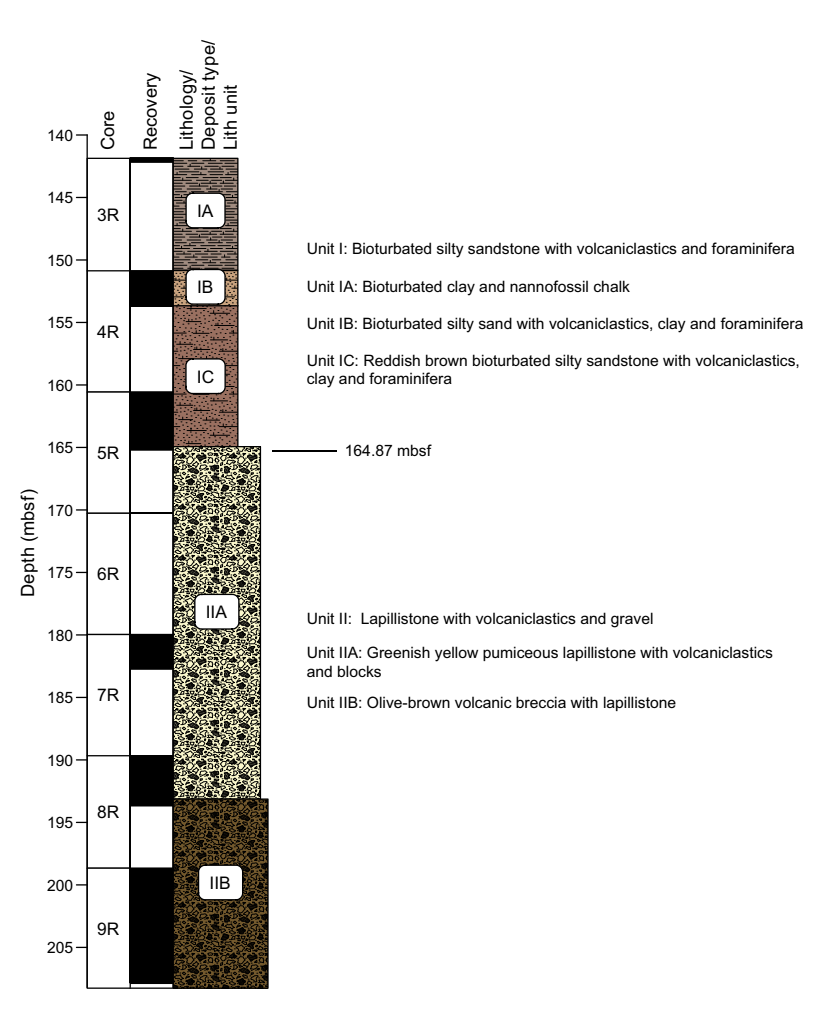


Figure F5. Lithostratigraphic synthesis, Site U1584.

sandy silt with clay and foraminifera (Lithostratigraphic Unit I; 142.10-164.84 mbsf) and a lower volcaniclastic-dominated (pumiceous) succession composed of greenish to brown pumice lapilli and varying content of fragmentary lithic volcanic lapilli and blocks, together with infrequent layers of moderately well-sorted scoriaceous ash and small lapilli with rare individual bioclasts toward the base (Lithostratigraphic Unit II; 164.84-207.75 mbsf). No igneous basement was encountered, and the hole was ended at 207.75 mbsf. In Unit I, core recovery increases with sediment consolidation downhole, from  $\sim 3\%$  in the chalk (Subunit 1A) to 30%-50% in the silty sandstone (Subunits IB and IC). In Unit II, core recovery increases with degree of cementation, from  $\sim 25\%-40\%$  in the greenish yellow pumiceous lapillistone (Subunit IIA) to >90% in the olive brown pumiceous lapillistone and volcanic breccia (Subunit IIB).

Unit I consists of a  $\sim$ 23 m thick succession of bioturbated clayey-nannofossil chalk passing downhole into highly bioturbated, pale brown to reddish silty sand with varying amounts of carbonate, with minor volcaniclastic intercalations including a few coarser beds of vitric and lithic ash. The unit is highly bioturbated throughout, effectively erasing any original bedding or sedimentary structures. Unit I was divided into three subunits based on significant compositional or color changes in the clayey-silty sand unit (i.e., rapid change from pale brown to reddish brown at the base of a tephra band in Section 397T-U1584A-4R-CC, 16 cm) together with a change to a finer more silt- and carbonate-rich composition.

- Subunit IA (142.10–150.80 mbsf) recovered 5 to 8 cm long pieces and gravel-sized fragments of consolidated pale pinkish gray bioturbated clayey-nannofossil chalk (CaCO<sub>3</sub> content = ~40%–60%) interpreted as a pelagic deposit.
- Subunit IB (150.80–153.64 mbsf) is a succession of consolidated/lithified pale brown clayey bioturbated silty sand, potentially up to  $\sim 10$  m thick, with volcaniclastics and foraminifera (CaCO<sub>3</sub> content =  $\sim 25\%$ –30%). This subunit is interpreted as background pelagic carbonate sedimentation with siliciclastic, silt-sized intervals deposited by turbidity currents.
- Subunit IC (153.64–164.84 mbsf) consists of  $\sim 11$  m of lithified reddish brown silty sandstone with foraminifera, volcaniclastic and clay components, and lower CaCO $_3$  content ( $\sim 20\%$ ). The subunit is heavily bioturbated with infrequent layers of moderately well sorted medium sand and gravel and rare shell bioclasts. The relative amount of background pelagic sedimentation decreases relative to siliciclastic, silt- to sand-sized deposition, possibly from turbidity currents.

Unit II consists of >43 m thick, dominantly volcaniclastic succession of lapillistone containing varying proportions of green to reddened (oxidized) pumice mixed with altered basaltic lithic fragments (see **Basaltic clast summary**). The boundary between Units I and II is abrupt but not preserved (Section 397T-U1584A-5R-4, 64 cm). Two subunits are recognized in Unit II based on a change in component proportions in the upper part of Core 5R and increasing downhole lithification by a mixture of interstitial altered ash and zeolite.

- Subunit IIA (164.84–193.60 mbsf) is a ~20 m thick unstratified succession of green pumice lapilli fragments with a downward increasing component of basaltic lithic fragments and irregular-shaped blocks set in a matrix of fine-grained gray ash-like material, calcite and zeolite. Two crudely graded intervals from coarser lapilli with volcanic blocks to smaller pumice lapilli with infrequent lapilli-sized basaltic volcaniclasts can be recognized.
- Subunit IIB (193.60–207.75 mbsf) is a >14 m thick lithified olive brown volcanic breccia consisting of unstratified oxidized pumiceous lapillistone and brown volcaniclastics with blocks in roughly equal proportions. The subunit is characterized by a downhole reduction in dominant clast size and a greater frequency of subrounded pumice lapilli with rare rounded, internally zoned lapilli; it has a greater bulk density than Subunit IIA (see **Physical properties**). Hole U1584A ended within this unit at 207.75 mbsf.

Deposition of the succession indicates a change from a volcaniclastic-dominated succession in which the main preserved eruptive products are highly vesicular pumice with basaltic lithic fragments and fine ash. Basaltic fragments include occasional cobble- or block-sized fragments. The degree of alteration and rounding of pumice clasts deceases upward, and observable crude layering may have been caused by eruptive pulsing. The later, overlying sediments are fine to medium

clayey sands passing upward into lower energy (deeper water?) ash clayey silts with a concomitant decrease in volcaniclastic component and finally into pelagic chalks with a minimal clastic component. These contain infrequent thin and dispersed ash (silt- and sand-sized) layers, most likely turbidites.

#### 4.1.3.1. Basaltic clast summary

In Unit II of Hole U1584A, basalt clasts range in diameter from <1 to 6 cm. These clasts show a range in mineralogy and porphyritic and aphanitic textures. No volcanic glass was observed. The highly phyric clasts typically contain abundant olivine phenocrysts (8%–10%) with some pyroxene (1%–3%). All olivine is partly to completely altered to iddingsite, and the pyroxenes display varying degrees of alteration. Moderately and sparsely phyric basalt clasts have lower olivine abundances (0%–7%) with more plagioclase phenocrysts (0%–5%). Pyroxene is often present in low amounts (0%–2%). Aphyric clasts are also present only as a minor component. Texturally, olivine is found as single crystals or small crystal clusters. Plagioclase phenocrysts range from blocky crystals to elongate crystals with variable degrees of alteration to sericite. Pyroxene is present in thin, tabular crystals with only minor visible alteration. Vesicle abundance varied widely, with some non-vesicular clasts and others containing up to 30% vesicles. Vesicles commonly contain alteration minerals ranging from a thin zeolite lining to being completely filled with calcite.

### 4.1.4. Biostratigraphy

Expedition 397T did not have any biostratigraphers on board, and we therefore have no data on the age of the sediments. Samples from Sites U1584 and U1585 were taken for a micropaleontological assessment after the expedition.

#### 4.1.5. Paleomagnetism

Cores from Hole U1584A did not offer much potential for accomplishing paleomagnetic objectives for Expeditions 391 and 397T. No basaltic basement was cored, and the section of basal sediments that might produce reliable paleomagnetic data was short. Much of the section was volcaniclastic breccia, which is expected to be a poor magnetic recorder because the glassy matrix has low magnetization and basalt clasts are randomly oriented, so no coherent inclination record can be obtained. Superconducting rock magnetometer (SRM) measurements were made on all available material (Cores 397T-U1584A-4R, 5R, and 7R–9R; Core 6R was empty). These measurements found that the basal sediments in Cores 4R and 5R, which contain calcareous clay and chalk, have moderate and coherent magnetization intensities, but deeper volcaniclastic cores have generally low intensities, interrupted by high intensity spikes from basalt clasts. Discrete sample measurements augment and reinforce this picture. The coherent magnetization in the calcareous clay unit gives a consistent positive magnetic inclination that is interpreted as recording a reversed magnetic polarity.

#### 4.1.6. Sediment geochemistry

Sediment samples were analyzed to determine  $CaCO_3$  wt%, total carbon (TC), total inorganic carbon, total organic carbon (TOC), and total nitrogen (TN). At Site U1584, seven samples were collected from Cores 397T-U1584A-3R through 5R. In Lithostratigraphic Subunit IA,  $CaCO_3$  content is moderate with a mean of  $55.7 \pm 15.6$  wt%. The mean  $CaCO_3$  content then decreases to  $23.7 \pm 3.7$  wt% and  $22.4 \pm 10.3$  wt% in Subunit IB and Subunit IC, respectively. TOC shows a general decrease from Subunit IA ( $0.26 \pm 0.1$  wt%) to Subunit IC ( $0.07 \pm 0.1$  wt%). Therefore, TC contents are nearly identical (within error) to total inorganic carbon. Subunit IA has subtly higher TC ( $6.5 \pm 1.5$  wt%) than Subunits IB and IC ( $3.2 \pm 0.5$  wt% and  $3.8 \pm 1.5$  wt%, respectively). TN contents are below the instrumental detection limits for all samples.

Four representative basalt clasts (4–6 cm) found in volcaniclastic sediment from Site U1584 were analyzed for major and select trace element compositions using inductively coupled plasma–atomic emission spectroscopy (ICP-AES). Three samples from Site U1584 are basalt, and one is basalt trachyandesite; all four samples are alkaline. The basalt clasts from Site U1584 have a narrow range of SiO<sub>2</sub> (45.02–46.40 wt%), TiO<sub>2</sub> (2.05–2.54 wt%), and K<sub>2</sub>O (1.46–1.73 wt%) but a wide range of MgO (2.23–9.50 wt%). The clasts span a range of Mg# (22.8–62.4) and show decreases in TiO<sub>2</sub>, Al<sub>2</sub>O<sub>3</sub>, and Sr and an increase in Ni with increasing Mg#. Although compositionally hetero-

geneous, Site U1584 samples all have higher  $K_2O$ ,  $Al_2O_3$ , Ni, and Sr than the samples from Expedition 391 sites.

### 4.1.7. Physical properties

Whole-round core logging included measurement of gamma ray attenuation (GRA) bulk density, pass-through magnetic susceptibility (MS), and natural gamma radiation (NGR). The whole-round section surfaces of igneous rocks and some breccias were also imaged in four quadrants. After splitting, the section halves were imaged and measured using the diffuse color spectrophotometer and a point-susceptibility meter. Discrete samples were measured for moisture and density (MAD) and *P*-wave velocity.

The results can be broken down into two categories based on how well they correlated with the two main lithostratigraphic units: mud and sand–dominated lithified sediment in Unit I and lapillistone in Unit II, with an increasing proportion of volcanic lithic fragments downhole. NGR, MS, point MS (MSP) and *P*-wave velocity correlated with the lithostratigraphic units, showing distinct changes between the units. NGR, MS, and MSP values increase slightly downhole from Subunit IB to Subunit IC, where they reach their highest relative values. Continuing downhole from Subunit IC to Subunit IIA, values decrease significantly from ~25 to 16 counts/s (NGR) and ~700 to 50 SI (MS and MSP). From the top of Subunit IIA through Subunit IIB, NGR, MS and MSP remain relatively constant, with a gradual decrease in their values toward the bottom of the hole. *P*-wave velocity behaves inversely to MS and NGR, increasing toward the bottom of Subunit IIB (from ~1770 to 3600 m/s). Bulk density measurements (GRA and MAD) and porosity remain consistent through the lithologic boundary. Density measurements stay consistent from Subunit IB through Subunit IIA and sharply increase going into Subunit IIB (from ~1.77 to 2.28 g/cm³). Porosity stays at its highest value from Subunit IB through Subunit IIA and decreases in Subunit IIB from ~56% to ~27%.

#### 4.2. Site U1585

#### 4.2.1. Background and objectives

Site U1585 was the second of two planned sites to sample the northern Walvis Ridge Guyot Province seamounts at locations slightly younger than that of the morphologic split, where the single ridge becomes two or three chains with different isotopic signatures. The site cores a Tristan track seamount that is part of a quasilinear chain of seamounts and ridges that stretch to the volcanically active Tristan da Cunha island group and have the same isotopic signature. The principal goal was to core basalt lava flows for major and trace element and isotope geochemistry, obtain fresh basalt samples for geochronology, and recover multiple lava units for paleomagnetic inclination studies. Other important science objectives were to learn more about the volcanological formation and evolution of Walvis Ridge seamounts and to obtain sediments that complement prior studies of sedimentation in the region.

#### 4.2.2. Operations

We completed the 111 nmi transit from Site U1584 to Site U1585 (proposed Site TT-04A) at a speed of 11.4 kt and arrived on 17 September 2022 at 1615 h (UTC + 1 h). Dynamic positioning mode was established, and we were ready for operations at 1650 h. A bit and bit sub were made up to the RCB BHA, which was deployed to just above the seafloor based on the PDR signal. We picked up the top drive, pumped the pig to clear the newly installed pipe from potential rust and other obstructions, dropped the RCB, and began to spud Hole U1585A. The mudline was established by advancing the BHA until the driller noted a tag and the core barrel was recovered with a muddy coating. At 0340 h on 18 September, we declared the seafloor depth at 3468.5 mbrf (3457.3 meters below sea level [mbsl]). At 0430 h, a wash barrel was dropped, followed by a center bit, and we drilled ahead to 144.1 mbsf. The wash barrel and center bit were retrieved at 1815 h, the core barrel was dropped, and coring began with Core 3R. The driller noted a hard tag at 250 mbsf, followed by a drilling break at 262 mbsf. This corresponded to the penetration of a massive basalt breccia layer. Hard rock drilling rates were encountered from Core 31R downward, corresponding to the penetration of massive basalt. The last core, 39R, was retrieved in the morning of 23 September, reaching a total penetration of 498.8 mbsf. In Hole U1585A, we recovered a total of 217.7

m of sediment and rock for a total of 354.7 m interval cored, with recovery ranging 11%-103% (average = 61%).

At 0615 h on 23 September, having used the available drilling time, we began retrieving the drill string, and the bit cleared the rig floor at 1555 h, ending Hole U1585A. The total time spent on this hole and Site U1585 was 143.3 h, or 5.97 days. The drill floor was secured, the thrusters were raised, and the voyage to Lisbon, Portugal, began at 1715 h. The 4333 nmi transit ended at 0950 h on 11 October when the pilot boarded the vessel. Expedition 397T ended at 1115 h when all lines were secured at the Rocha cruise terminal, Port of Lisbon, Portugal.

COVID-19 mitigation protocols were followed with mask wearing, social distancing, and antigen testing of all personnel for the 6 days that started after the last recorded positive case on board was isolated, as mandated by the shipboard COVID-19 mitigation protocol. As of midnight on 21 September, daily COVID-19 testing ended and wearing of masks was no longer mandatory. On 24 September, the last of four infected personnel was released from isolation.

## 4.2.3. Lithostratigraphy

A 274 m thick succession consisting of a mixture of pelagic and detrital sediment and mixed fine (argillaceous) to coarse (blocky) volcaniclastic materials lying on top of 81 m of igneous basement was drilled at Site U1585 (Figure **F6**). Igneous basement was encountered at 417.65 mbsf, and the hole was ended at 498.8 mbsf. Five main lithostratigraphic units were recognized, four in the sediment section and one in the igneous section.

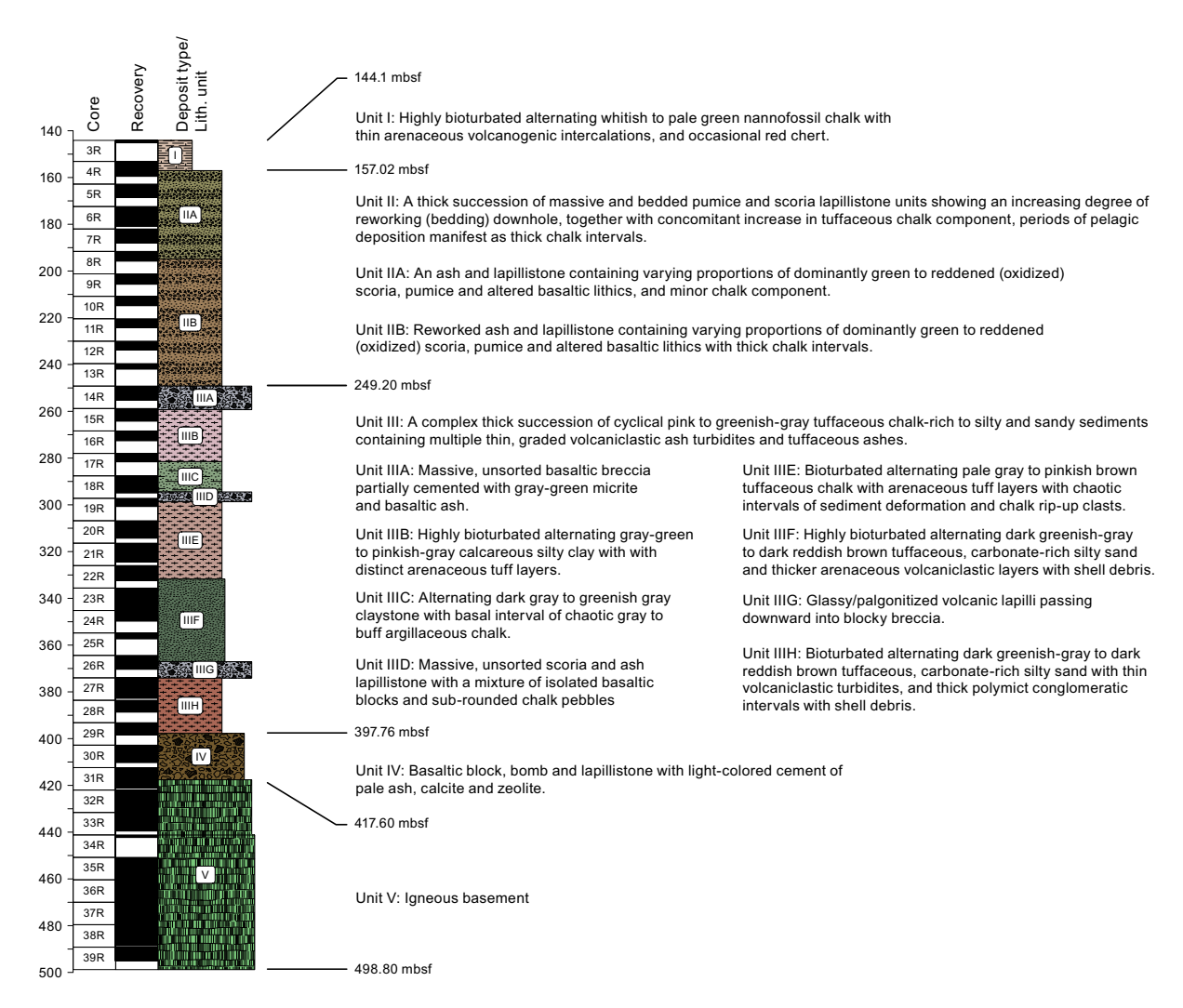


Figure F6. Lithostratigraphic synthesis, Site U1585.

Unit I (144.10-157.02 mbsf) is a  $\sim 13$  m succession of bioturbated nannofossil chalk with foraminifera, faintly alternating in color from whitish to pale green, with chert horizons and containing occasional thin ash intercalations.

Unit II (157.02-249.20 mbsf) is a thick  $(\sim 92 \text{ m})$  succession of massive and bedded pumice and scoria lapillistone units showing a downhole increasing abundance of basaltic clasts, reworking and compaction. It is divided into two subunits (IIA and IIB) based on increasing reworking, clast alteration, and tuffaceous chalk intercalations.

- Subunit IIA (157.02–194.80 mbsf) is a massive, unsorted basaltic lapillistone of dominantly pale green pumice, scoria, and basaltic clasts.
- Subunit IIB (194.80–249.20 mbsf) is a continuation of Subunit IIA but displays an increasing degree of reworking and clast oxidation and chalk intercalations.

Unit III (249.20–397.76 mbsf) is a thick (~149 m), complex succession of alternating pink to greenish gray tuffaceous chalk-rich to silty and sandy sediments containing multiple thin, graded ash turbidites and tuffaceous ash; intercalated thick tuffaceous chalk intervals, occasionally slumped; and several thick, coarse lapilli- and block-dominated volcaniclastic layers. It is divided into eight subunits (IIIA–IIIH). Three of these (IIIA, IIID, and IIIG) are mainly basalt breccias.

- Subunit IIIA (249.02–259.29 mbsf) is a >10 m thick unsorted, partially cemented basalt-dominated volcanic lapillistone breccia with basaltic ash.
- Subunit IIIB (259.29–281.50 mbsf) is a uniform, >22 m thick, highly bioturbated gray green to pinkish gray tuffaceous chalk and silty clay with some graded pumice and ash layers.
- Subunit IIIC (281.5–294.48 mbsf) is a ~13 m thick bioturbated sequence of alternating dark gray to greenish gray tuffaceous, chalky claystone displaying downhole disturbance including inclined bedding, rounded chalk clasts, and brittle fracturing.
- Subunit IIID (294.48–298.67mbsf) is a ~4 m thick basalt-dominated volcanic lapillistone
  breccia consisting of densely packed scoria and basalt with a mixture of tuffaceous chalk
  pebbles and isolated basaltic blocks toward its base.
- Subunit IIIE (298.6–331.76 mbsf) is a ~33 m thick complex succession of bioturbated tuffaceous chalk displaying pale gray to pinkish brown color alternations and infrequent tuff or ash layers, some preserving plagioclase crystals and bioclasts. Its base contains chaotic intervals displaying soft-sediment deformation with rip-up clasts, indicative of submarine slumping.
- Subunit IIIF (331.76–367.07 mbsf) is a >35 m succession of carbonate-rich silty clay with a downhole increase in grain size to a highly bioturbated, dark reddish brown to dark greenish-gray silty sand. The frequency of crystal-rich ash and shell debris layers increases downhole, indicative of shallower water.
- Subunit IIIG (367.07–374.10 mbsf) is a >7 m thick polymict lapilli-sized volcanic breccia passing downward into blocky breccia with minor reworking. It contains zoned (accretionary?) lapilli and basalt fragments with glassy/palagonitized (tachylitic) rims. These juvenile pyroclasts indicate proximity to a volcanic source.
- Subunit IIIH (374.10–397.76 mbsf) is >24 m thick succession. The uppermost interval is a bioturbated dark greenish gray to dark reddish brown tuffaceous, carbonate-rich silty clay with numerous ~2–5 cm thick tuff or ash layers. The lower half of the unit contains thicker (~5–10 cm) polymict conglomeratic graded intervals containing tuffaceous chalk pebbles, fine shell debris, and lapillistone with some block-sized clasts. Lapillistone contains a palagonitized quenched/glassy basaltic fragments, an admixture of juvenile pyroclastic fall-out.

Unit IV (397.76–417.60 mbsf) is a thick (~20 m) deposit of volcanic breccia consisting of a stacked succession of basaltic block, bomb, and accretionary lapilli. An abundance of glassy shards and tachylitic rims on angular basaltic fragments, together with marine bioclasts and recrystallized foraminifera in the cement, indicates juvenile and reworked volcaniclastic components and a complex explosive eruptive–sedimentary environment. It is not divided into subunits.

In chronological order, the cored succession begins with an igneous basement consisting of unusually thick uniform basaltic units (Unit V). This is overlain by a varied succession combining initially juvenile volcaniclastic material (Unit IV) and subsequent sedimentary lithofacies involving reworked volcaniclastics eventually passing into deep marine chalk-dominated sedimentary

units (Units I–III). The lowermost basalt flow and primary volcanic deposits represent the final stages of the constructive phase of the evolution of the volcanic edifice. Following this effusive-explosive phase is a period of deepening marine environment and the onset of drowning of the site (Unit III). Repeated influxes of coarse volcanic debris indicate a nearby offshore, shallow source in which accumulated clastic detritus periodically slumped into deeper water. Long periods of deepwater pelagic accumulation are represented by the preservation of alternating redox conditions within tuffaceous and increasingly purer nannofossil chalk sediments (Subunits IIIB and IIIE). Tuffaceous carbonates eventually give way to more homogeneous carbonate ooze (chalk). The thick pumice- and scoria-rich layers of Unit II represent a much later and entirely separate phase of volcanism. The length of hiatus between this later eruptive phase and the emplacement of the earlier lava units remains to be determined.

#### 4.2.4. Igneous petrology and volcanology

Site U1585 penetrated 81.2 m of igneous basement (interval 397T-U1585A-31R-5, 75 cm, to 39R-6, 43 cm) with 70.2 m recovered (86%) (Figure F7). The igneous basement at Site U1585 is designated Lithostratigraphic Unit V, and Hole U1585A terminates within a massive lava flow with a minimum flow thickness of 43.3 m. Three igneous lithologic units were identified at Site U1585. Unit 1 and Unit 3 consist of massive lava flows, and each have two subunits distinguished by distinct textural and mineralogical changes. Unit 2 is an igneous unit that consists of a mineralogically and texturally distinct piece of quenched lava potentially related to a pillow sequence with very low recovery.

Igneous Unit 1 is a sparsely to highly phyric olivine-clinopyroxene  $\pm$  plagioclase massive basalt (interval 397T-U1585A-31R-5, 75 cm, to 34R-1, 0 cm; 417.60–441.2 mbsf). Textural and mineralogical changes suggest that this unit likely consists of, at minimum, two basalt flows, each with distinctive mineralogy. The topmost flow (Subunit 1a) is a 4.47 m thick (417.60–422.07 mbsf) massive flow. Subunit 1b is a 19.1 m thick (422.07–441.20 mbsf) massive flow that is more fractionated (moderately clinopyroxene  $\pm$  plagioclase phyric) basalt with noticeably coarser ground-mass crystals than Subunit 1a.

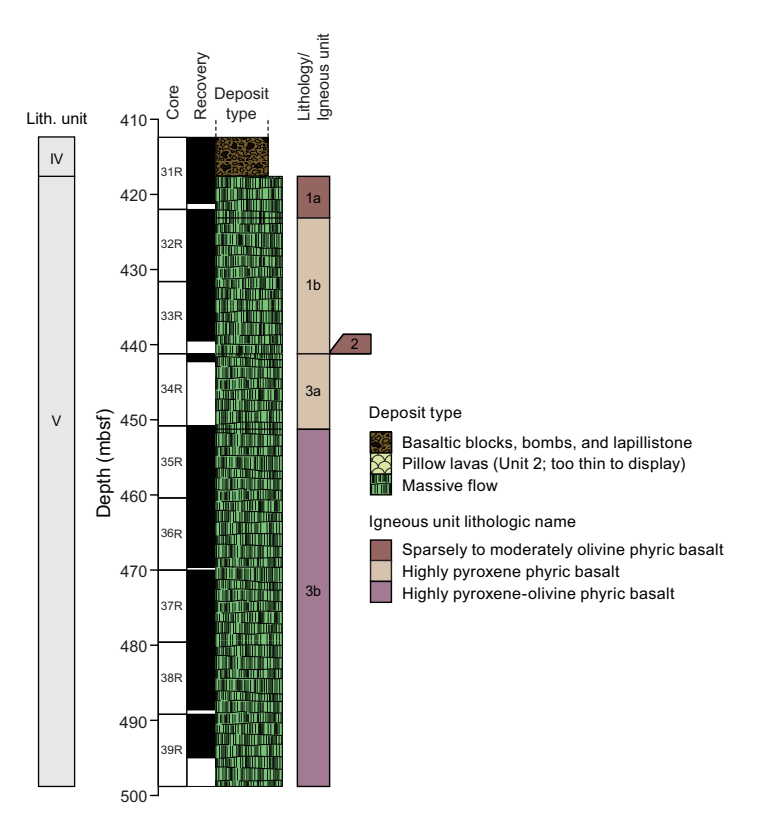


Figure F7. Stratigraphic column illustrating recovery of igneous basement, Hole U1585A.

Igneous Unit 2 consists of a 3 cm (441.20–441.23 mbsf) piece of quenched basalt with olivine phenocrysts in a microcrystalline groundmass. Because unrecovered intervals are defined by the end of a core, the thickness of Unit 2 is underrepresented and the thickness for Subunit 3A is overrepresented.

Igneous Unit 3 consists of two massive lava flows without any clear flow boundary features. However, changes in texture, mineralogy, and geochemistry suggest that two flows with separate fractionation histories may be present. The first flow is identified as Subunit 3a. It is 10.3 m thick (441.23-451.26 mbsf) and consists of a highly phyric clinopyroxene-plagioclase massive basalt flow with a fine-grained groundmass. Subunit 3b is a thick (>43.7 m; 451.26-495.0 mbsf), relatively featureless massive basalt flow that is moderately to highly pyroxene-plagioclase  $\pm$  olivine phyric.

Broadly, two stages of alteration can be identified intermittently throughout the igneous units: (1) a higher temperature alteration chlorite-sericite-zeolite facies and (2) a subsequent, lower temperature Fe oxyhydroxide alteration. The higher temperature alteration was more pervasive and resulted in pyrite, calcite, chlorite, and zeolite filling vesicles, veins, and fractures. The intensity of this alteration was moderate through Unit 1 and Subunit 3a but decreased in intensity toward the bottom of Subunit 3b. The low-temperature, more oxidizing episode of alteration is patchy and often seen localized around fractures, which provided fluid pathways. The more oxidizing alteration episode happened secondarily and often removed vesicle and vein filling. It was observed mostly in Unit 1.

#### 4.2.5. Paleomagnetism

Almost all core sections were measured with the SRM, producing 52,829 measurements. Additionally, 125 discrete samples were treated to detailed demagnetization. Magnetization intensity within the sedimentary section displayed an extreme range  $(3.0 \times 10^{-5} \text{ to } 7.3 \text{ A/m})$  because of the variation from weakly magnetic carbonate sediments to basalt breccia (Figure F8). Magnetization intensity of basalt flow cores ranged 0.45-15.26 A/m, which is normal for relatively unaltered basalt (Figure F9). Although a few of the upper breccia units (Subunits IIB and IIIA) gave scattered paleomagnetic inclination data, most cores produced consistent results. Cores 397T-U1585A-18R through the basalt section to the bottom of the hole yielded positive inclinations, implying reversed magnetic polarity. The calcareous sediments at the top of the cored interval, Cores 3R and 4R (Unit I), are also reversed. In between there is at least one but perhaps two normal polarity zones, depending on confirmation of an intervening reversed interval. Cores 13R and 14R and the top of Core 15R gave scattered inclination data, but detailed demagnetization of two discrete samples indicates reversed polarity. This polarity zone requires confirmation with later study. If confirmed, it divides normal polarity zones observed in Cores 9R-12R and 15R to the top of Core 18R. If not, there is probably only one normal polarity interval. The occurrence of a magnetic reversal in the latter core provides a potential opportunity for dating that can help calibrate the magnetic reversal time scale. Isothermal remanent magnetization studies show that the magnetization carriers in the sediments are mostly titanomagnetite, but they have varying amounts of high coercivity mineral, likely hematite. These experiments also show that the magnetizations of some massive flows are soft and may be carried by large, multidomain grains.

#### 4.2.6. Sedimentary geochemistry

A total of 119 sediment samples from Lithostratigraphic Units I–III were analyzed to determine the  $CaCO_3$  wt%, total carbon (TC), total inorganic carbon, total organic carbon (TOC), and total nitrogen (TN). In Unit I,  $CaCO_3$  content is high with a mean of 77  $\pm$  9.7 wt%. The mean  $CaCO_3$  content is more moderate in Subunits IIB, IIIA, IIIB, and IIIE, ranging 40  $\pm$  9.1 wt% to 62.9 wt% (numbers with  $\pm$  values are averages with standard deviation; those without are single measurements). Subunits IIA, IIIF, and IIIH all have low  $CaCO_3$ , ranging 26–31 wt%. TOC content is low across all lithologic units (<0.5 wt%) and shows no consistent trend between units. Therefore, TC contents are nearly identical (within error) to total inorganic carbon and do not show a clear pattern with depth. Likewise, given the complexity of each lithostratigraphic unit, it is difficult to draw clear connections between TC and lithostratigraphic units. Subunit IA and IIA have relatively higher TC (7.9 and 9.3  $\pm$  1.3 wt%, respectively) than other units. TC is moderate in Subunits

IIB, IIIB, IIIC, IIIE, and IIIH (4.0–6.6 wt%) and low in Subunits IIA, IIID, and IIIF (2.8–3.1 wt%). TN contents are below the instrumental detection limits for all samples.

### 4.2.7. Igneous geochemistry

At Site U1585, 16 samples were analyzed for major and trace elements via ICP-AES from the two igneous units comprised of massive flows. Additionally, 13 samples from large basalt clasts within various volcaniclastic lithostratigraphic units above the igneous basement were also analyzed. The majority of Site U1585 basalt clasts and lava flows lie within the basalt compositional field. However, five lava flows and three clasts are compositionally trachybasalts, and one basalt clast is a basaltic trachyandesite. Apart from three transitional basalt clasts, all Site U1585 samples are alkaline. Calculated Ti/V values demonstrate that the basalt lava flows have higher Ti/V values than most of the basalt clasts. The lower Ti/V values are consistent with lavas from Expedition 391 Sites U1575–U1577 and overlap with values from MORB and the transition to oceanic island basalt (OIB). The higher Ti/V values associated with the basalt lava flows fall between the values from Sites U1575–U1577 and Site U1578. They also lie completely in the OIB field.

The basalt clasts from Site U1585 show a wide range of Mg# (32.5–64.6), similar to basalt clasts from Site U1584. However, unlike clasts from Site U1584, the more numerous basalt clasts from Site U1585 also show a wider range of other elemental abundances (e.g.,  $SiO_2 = 45-52$  wt%; CaO = 5.0-16.6 wt%;  $TiO_2 = 0.9-2.8$  wt%). The scatter in  $K_2O$  may be due to seawater alteration. In contrast, the basalt lava flows show a range of compositions forming clear trends generated by fractional crystallization. The basalt lava flows show increasing  $SiO_2$ ,  $TiO_2$ , CaO,  $K_2O$ ,  $Al_2O_3$ , Zr, V,

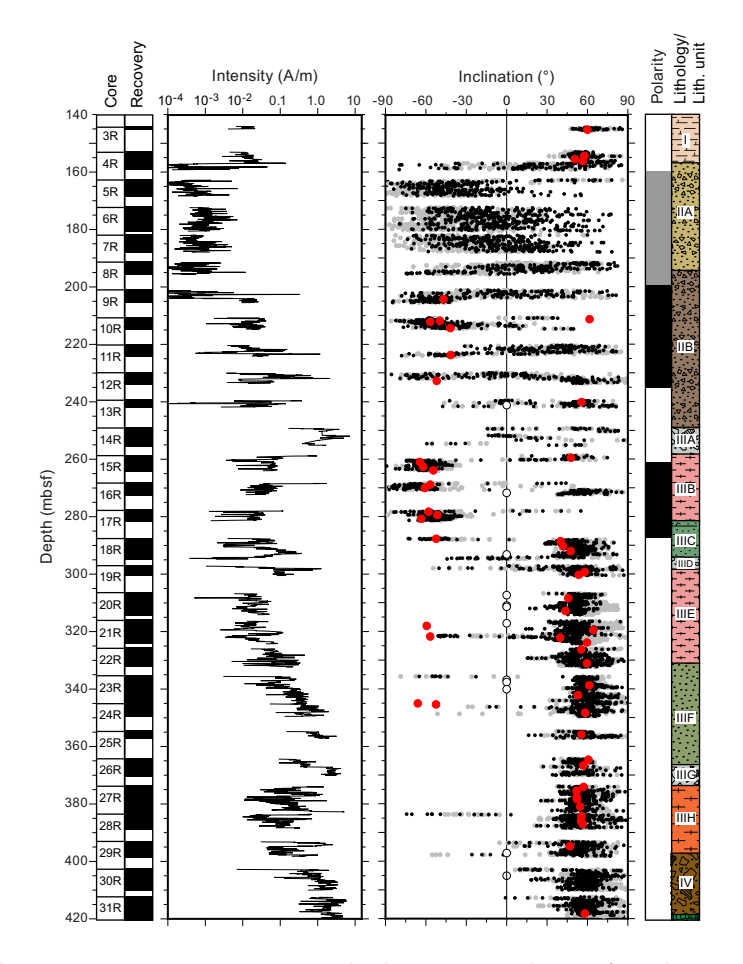


**Figure F8.** Natural remnant magnetization intensity and paleomagnetic inclination for sediment cores, Hole U1585A. Intensity is shown on a logarithmic scale. Inclination: gray dots = NRM, black dots = after 20 mT alternating field (AF) demagnetization, red dots = discrete cube samples, open symbols on the zero line = samples that did not produce satisfactory demagnetization results. Magnetic polarity: black = normal, white = reversed, gray = cannot be determined. See Figure F6 for lithology legend.

and Sr with decreasing Mg#. The strong positive correlation between Mg# and Ni are indicative of modest olivine accumulation in the most MgO-rich samples (up to 18.3 wt% MgO and 565 ppm Ni). Overall,  $TiO_2$  contents are modest for both basalt clasts and basalt lava flows; none are as  $TiO_2$ -rich as Site U1578 lavas. However, the  $TiO_2$  content of the basalt clasts are lower than those of the basalt lava flows with similar Mg#. The relational offset is also observed in Zr and Sr. This compositional difference between the younger basalt clasts and the older basalt lava flows may be due to a change in magmatic source.

### 4.2.8. Physical properties

In Hole U1585A, three primary sedimentary units were identified and defined by changes in sedimentary successions and major shifts in physical property behavior. Three units were also identified within the igneous basement, but those units had minor changes in physical properties and were mainly distinguished using changes in petrography and geochemistry.

The physical properties data can be broken down into two categories: (1) properties that mark major lithostratigraphic boundaries by displaying distinct changes from the previous unit and (2) properties that display intraunit variation and small-scale variations (e.g., within a single core). Bulk density measurements based on GRA and MAD analysis and *P*-wave velocity fall within the first category and were best suited to identify major lithostratigraphic unit boundaries. Bulk density and *P*-wave velocity are nearly homogeneous in Units I–III, excluding the basalt breccia units in Unit III (Subunits IIIA, IIID, and IIIG), where *P*-wave velocity displays higher peaks. The two properties were more variable in Unit IV due to the amount of basaltic blocks within the ash-cemented lapillistone but stabilized and steadily increased into the igneous basement to the bot-

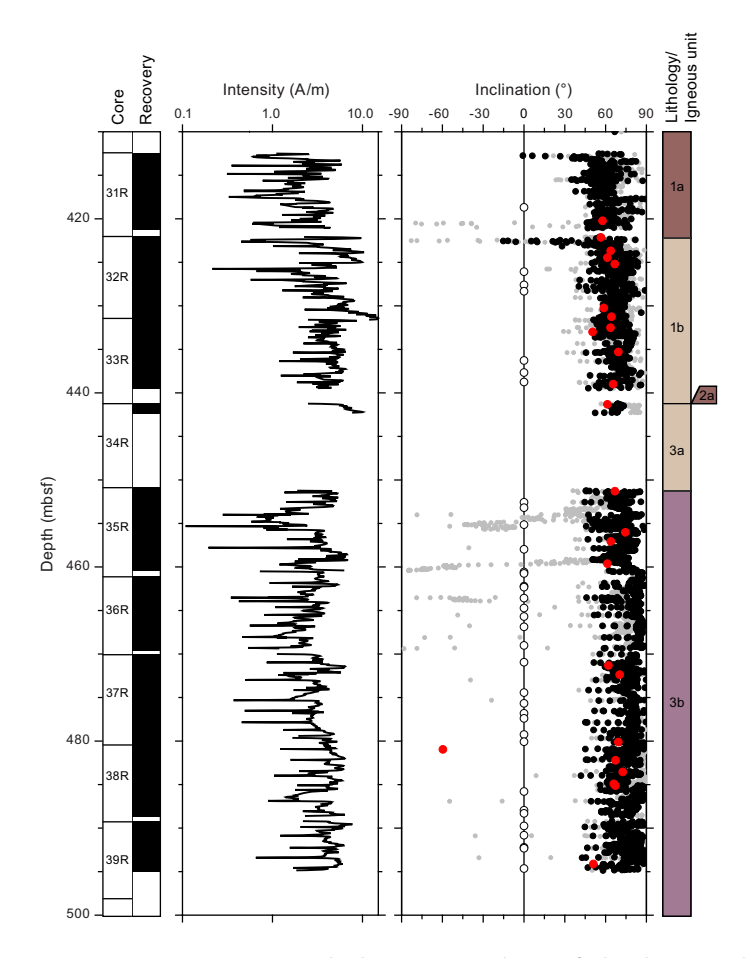


**Figure F9.** Natural remnant magnetization intensity and paleomagnetic inclination for basalt cores, Hole U1585A. Intensity is shown on a logarithmic scale. Inclination: gray dots = NRM, black dots = after 20 mT alternating field (AF) demagnetization, red dots = discrete cube samples, open symbols on the zero line = samples that did not produce satisfactory demagnetization results. Section is entirely reversed polarity. See Figure F7 for lithology legend.

tom of the hole. MS, MSP, NGR, and porosity have more interunit variation when compared to density and *P*-wave velocity. They display systematic changes within a single core. Core-section (meter-scale) variations are present, but careful processing of the data is needed to remove outliers introduced by gaps between sections and pieces. In general, both MS and NGR steadily increase from the top of the hole within the chalky Unit I to the base of breccia Unit IV, and both display intraunit variations on meter and core length scale that fluctuate between different sediment successions. NGR decreases a small amount in the highly phyric pyroxene-olivine basalt of Igneous Subunit 3b. Porosity was measured only in Units I–III and varies between 40 and 60 vol% across lithostratigraphic units and within single cores.

# 5. Preliminary scientific assessment

Expedition 397T was designed to address the loss of two sites during Expedition 391. Two major objectives of Expedition 391 were (1) to core a transect in the northern Guyot Province to recover basalt lava flows from one volcano each of the Tristan, Center, and Gough tracks to better understand the isotopic zonation present at the DSDP Leg 74 transect farther north and (2) to use paleomagnetic measurements from these flows to determine a precise paleolatitude. Additional objectives were to obtain precise radiometric dates and to better understand the volcanological evolution of Guyot Province seamounts.

Expedition 391 cored Hole U1578A deep into volcanic basement, producing a set of cores that was close to ideal. The  $\sim$ 300 m section spanned a long time period, with lava flows interspersed with numerous pelagic and volcaniclastic intervals. Moreover, the flows rendered many glassy margins (excellent for geochemistry and isotopic chemistry) and included interesting changes in geochemistry and fresh intervals rich in olivine (a mineral critical to some geochemical studies). In a sports analogy, Hole U1578A was a home run. Given that the original pre-Expedition 391 operational time estimates for drilling at proposed Sites GT-4A and TT-4A was a total of 9.3 days, having only 7 days of drilling time allotted for Expedition 397T suggests that it is unfair to compare the results of Sites U1584 and U1585 with those of Hole U1578A. It was always likely that operational or geological problems would cut into that time, meaning less scientific output. Overall, Expedition 397T came up a little short on one hole, U1584A, but did well on another, Hole U1585A, even if the latter was significantly different from Hole U1578A. On the whole, Expedition 397T did indeed provide useful samples that will help achieve the goals of Walvis Ridge Hotspot drilling.

## 5.1. Hole U1584A

Hole U1584A on the Gough track guyot recovered only a short interval of calcareous sediments overlying three cores of volcaniclastics containing generally small basalt clasts. Because of its inauspicious beginning, drilling in Hole U1584A was terminated early to save the time for drilling elsewhere. The character of volcanic basement at all locations on the site survey seismic lines was the same (smooth), so there was no better place to core on the Gough track guyot.

Because the basalt clasts are small and encased in porous volcaniclastics, the clasts are altered to varying degrees. This limits their utility for geochemical and geochronological study. Expedition 397T scientists are, however, hopeful that useful geochemical data can be produced and that at least one reliable radiometric age can be determined. The time span is likely to be limited, and because the material was produced by explosive eruption(s) at the end of the guyot's formation, the material may not represent the original edifice construction (i.e., it may be a late-stage eruption). Nevertheless, any information about the geochemical signature and timing of the volcanic eruption will be useful for understanding the formation of Walvis Ridge and its guyots. Because the basalt clasts are jumbled in their volcaniclastic setting, they are useless for paleolatitude study.

#### 5.2. Hole U1585A

Hole U1585A encountered a volcanic section consisting of  $\sim$ 274 m of volcaniclastic material overlying  $\sim$ 81 m of basalt in the form of thick, massive flows. The basalt section was disappointing because it probably spans a limited time, is relatively homogeneous, contains little glass, and is moderately altered. These conditions mean that it may not serve for some geochemical studies

and may have limited variability and time span to average paleomagnetic secular variation or provide a record of time changes in the magma source. Nevertheless, there is abundant material that is likely to give some important geochemical data and a reliable radiometric date. Some parts of the flows contain fresh olivine, but the crystals are small, so geochemists will have some difficulty separating them out. The sediment section above the basalt is highly varied and contains intervals of abundant volcanic clasts and occasional glass. Moreover, it clearly spans a significant time interval. Thus, there is potential for producing interesting geochemical data as well as radiometric dates. In other words, the section is not as ideal as that from Site U1578, but it has some potential to produce important results.

From a volcanological perspective, the recovered sections are quite interesting. The volcaniclastic cores contain a record of material shed from the volcanic high, potentially spanning a significant period of the late stages of volcano construction. The cores suggest that the deeper, older section was deposited in shallow water, but that the higher, younger parts were deposited in deeper water. This transition implies emplacement over a long time interval as the volcano subsided beneath the sea surface. Several magnetic reversals were captured in the sedimentary section, providing more evidence of significant time passage. The basalt flow section is also interesting, even though likely limited in age range. Encountering thick, massive flows on the lower flanks of the seamount was unexpected. Seamount volcanism is typically characterized by low-effusion pillow lavas. Also unexpected were some internal geochemical and paleomagnetic variations within the flows that suggest later intrusion(s) and magma evolution. Thus, Hole U1585A may provide important data for understanding seamount volcanism in general and Walvis Ridge guyot volcanism in particular.

It is unclear how useful the Hole U1585A cores will be for paleolatitude studies. The hope was to core multiple lava flows, which would provide multiple samples of the paleomagnetic field over enough time to average paleosecular variation. Paleomagnetists consider lava flows to be a better magnetic recorder than most sediments. The cored basalt section probably spans a limited time interval, so it will not provide the desired result. It may be possible to obtain one or a few estimates of paleomagnetic inclination that can be combined with data from Hole U1578A. In contrast, the sediment section may provide useful data, but it displays complex lithologic changes that will require a significant effort to understand which units have been reworked and the ability of magnetic minerals to record the geomagnetic field. Nevertheless, shipboard results suggest that two to three magnetic polarity zones were sampled, so there is a significant time span. Because some paleomagnetists distrust sediment samples for paleolatitude study, the trick will be to produce data that are convincingly reliable.

# 5.3. Why did we not core the expected geology?

One may wonder why coring encountered volcaniclastics at both sites instead of the desired basalt. One part of the answer is that they may be hard to tell apart, but the rest of the answer is underinvestment in site survey seismic data. At both sites, acoustic basement (i.e., the deepest strong reflector beneath which little is seen) had the expected characteristic. Beneath sediments with only weak internal reflections, basement was a strong reflector and few coherent reflections occurred below. One may expect lava flows to create strong, undulating reflectors with diffractions and poor lateral continuity owing to the rough nature of lava flow surfaces. In the case of Site U1584, basement appears smooth, but it is on the flank of a volcano where significant volcaniclastic accumulation would not be expected. In addition, this character was seen on all of the few seismic lines over the target Gough track guyot. In hindsight, it appears that this volcano produced significant explosive eruptions covering its flanks with volcaniclastics. In a world where funds for geophysical data acquisition are less limited, perhaps other seismic profiles over nearby seamounts could have been acquired, giving an option without volcaniclastic cover.

Site U1585 appeared to be a better bet because the site is on the lower flank, away from summit eruptions, and the acoustic basement is strong and undulating, as would be expected. Site U1578 was in a similar location on a Center track guyot lower flank. It was poor luck that Site U1585 was covered with  $\sim$ 274 m of volcaniclastic-rich sediments and the lava flows were massive. The drill bit performed well and the hole gave no problems, so had we had more time, we could have drilled deeper, perhaps below the massive flows. We simply ran out of time to go deeper.

# 6. Connections to the 2050 Science Framework

Originally submitted during 2007, the Walvis Ridge hotspot drilling proposal was developed from the recommendations of the 2007 Hotspot Geodynamics Detailed Planning group (Duncan et al., 2007). This advisory group recommended drilling several hotspot seamount chains to leverage then new results from the Hawaiian-Emperor chain drilling. The proposal matured under the guidance of the IODP Science Plan 2013–2023 (Bickle et al., 2013) and mainly addresses the theme "Earth Connections: Deep processes and their impact on Earth's surface environment" because the project cored volcanic hotspot seamounts to understand the sources of hotspot magmas and their evolution through time. In particular, the project addressed "Challenge 8: What are the composition, structure, and dynamics of Earth's upper mantle?" and "Challenge 9: How are seafloor spreading and mantle melting linked to ocean crustal architecture?" Moreover, because Expeditions 391 and 397T sought to better understand the processes of submarine volcanism, both expeditions also addressed volcanic geohazards, and thus the theme "Earth in Motion: Processes and hazards on human time scales." More specifically, such knowledge fits "Challenge 12: What mechanisms control the occurrence of destructive earthquakes, landslides, and tsunamis."

Now under the guidance of its third planning document, the 2050 Science Framework for scientific ocean drilling (Koppers and Coggon, 2020) knowledge produced by Expeditions 397T and 391 address the strategic objectives "The Oceanic life cycle of tectonic plates" and "Feedbacks in the Earth system" because hotspot volcanism augments oceanic plates and modifies their behavior and evolution. In addition, the flux of melts from the upper mantle to the plates affects the surface and surface environments. Expeditions 391 and 397T also address the Flagship Initiative "Probing the deep Earth" because geochemistry of hotspot magmas can give clues about mantle plume source regions in the deep mantle. Moreover, studies of paleolatitude from paleomagnetic data gives clues about the evolution of mantle heterogeneities and their geodynamic effects on spin axis stability or mobility.

# References

Bickle, M., Arculus, R., Barrett, P., DeConto, R., Camoin, G., Edwards, K., Fisher, F., Inagaki, F., Kodaira, S., and Ohkouchi, N., 2011. Illuminating Earth's Past, Present and Future The Science Plan for the International Ocean Discovery Program 2013-2023: Washington, DC (Integrated Ocean Drilling Program). <a href="http://www.iodp.org/about-iodp/iodp-science-plan-2013-2023">http://www.iodp.org/about-iodp/iodp-science-plan-2013-2023</a>

Class, C., Koppers, A., Sager, W., and Schnur, S., 2015. Walvis Ridge-Tristan-Gough, South Atlantic—triple-zonation of a plume over 60 Ma and role of LLSVP. Presented at the Goldschmidt Conference Prague, Czech Republic, 16–21 August 2015. https://goldschmidtabstracts.info/2015/568.pdf

Courtillot, V., Davaille, A., Besse, J., and Stock, J., 2003. Three distinct types of hotspots in the Earth's mantle. Earth and Planetary Science Letters, 205(3–4):295–308. https://doi.org/10.1016/S0012-821X(02)01048-8

Creveling, J.R., Mitrovica, J.X., Chan, N.H., Latychev, K., and Matsuyama, I., 2012. Mechanisms for oscillatory true polar wander. Nature, 491(7423):244–248. https://doi.org/10.1038/nature11571

Doubrovine, P.V., Steinberger, B., and Torsvik, T.H., 2012. Absolute plate motions in a reference frame defined by moving hot spots in the Pacific, Atlantic, and Indian oceans. Journal of Geophysical Research: Solid Earth, 117(B9):B09101. https://doi.org/10.1029/2011JB009072

Duncan, R., Hanyu, T., Harada, Y., Harpp, K., Hoernle, K., Kellogg, L., Koppers, A., Sager, W., Steinberger, B., Tarduno, J., and Xu, Y.-G., 2007. Report from the Hotspot Geodynamics Detailed Planning Group: https://www.iodp.org/docs/workshops/325-hotspot-geodynamics-detailed-planning-group-dpg-report-jan-

nttps://www.ioap.org/docs/worksnops/325-notspot-geodynamics-detailed-planning-group-dpg-report-january-2007/file

Duncan, R.A., 1981. Hotspots in the Southern Oceans—an absolute frame of reference for motion of the Gondwana continents. Tectonophysics, 74(1–2):29–42. https://doi.org/10.1016/0040-1951(81)90126-8

Gold, T., 1955. Instability of the Earth's axis of rotation. Nature, 175(4456):526–529. https://doi.org/10.1038/175526a0

Goldreich, P., and Toomre, A., 1969. Some remarks on polar wandering. Journal of Geophysical Research, 74(10):2555–2567. https://doi.org/10.1029/JB074i010p02555

Gordon, R.G., 1987. Polar wandering and paleomagnetism. Annual Review of Earth and Planetary Sciences, 15(1):567–593. https://doi.org/10.1146/annurev.ea.15.050187.003031

Gordon, R.G., and Cape, C.D., 1981. Cenozoic latitudinal shift of the Hawaiian hotspot and its implications for true polar wander. Earth and Planetary Science Letters, 55(1):37–47. https://doi.org/10.1016/0012-821X(81)90084-4

Gordon, R.G., Woodworth, D.T., Gaastra, K., and Seidman, L.E., 2019. Paleogene true polar wander, origin of the Hawaiian-Emperor Bend, paleolatitude of Ellesemere Island and Cenozoic climate change. Presented at the Geological Society of American Annual Meeting, Phoenix, AZ, 22–25 September 2019.

- Hoernle, K., Rohde, J., Hauff, F., Garbe-Schönberg, D., Homrighausen, S., Werner, R., and Morgan, J.P., 2015. How and when plume zonation appeared during the 132Myr evolution of the Tristan Hotspot. Nature Communications, 6(1):7799. https://doi.org/10.1038/ncomms8799
- Homrighausen, S., Hoernle, K., Geldmacher, J., Wartho, J.A., Hauff, F., Portnyagin, M., Werner, R., van den Bogaard, P., and Garbe-Schönberg, D., 2018. Unexpected HIMU-type late-stage volcanism on the Walvis Ridge. Earth and Planetary Science Letters, 492:251–263. https://doi.org/10.1016/j.epsl.2018.03.049
- Homrighausen, S., Hoernle, K., Hauff, F., Wartho, J.A., van den Bogaard, P., and Garbe-Schönberg, D., 2019. New age and geochemical data from the Walvis Ridge: the temporal and spatial diversity of South Atlantic intraplate volcanism and its possible origin. Geochimica et Cosmochimica Acta, 245:16–34. https://doi.org/10.1016/j.gca.2018.09.002
- Homrighausen, S., Hoernle, K., Zhou, H., Geldmacher, J., Wartho, J.-A., Hauff, F., Werner, R., Jung, S., and Morgan, J.P., 2020. Paired EMI-HIMU hotspots in the South Atlantic—starting plume heads trigger compositionally distinct secondary plumes? Science Advances, 6(28):eaba0282. https://doi.org/10.1126/sciadv.aba0282
- Kono, M., 1980. Paleomagnetism of DSDP Leg 55 basalts and implications for the tectonics of the Pacific Plate. In Jackson, E.D., Koisumi, I., et al., Initial Reports of the Deep Sea Drilling Project. 55: Washington, DC (US Government Printing Office), 737–752. https://doi.org/10.2973/dsdp.proc.55.135.1980
- Koppers, A., and Coggon, R. (Eds.), 2020. Exploring Earth by Scientific Ocean Drilling: 2050 Science Framework: San Diego, CA (UC San Diego Library). https://doi.org/10.6075/J0W66J9H
- Koppers, A.A.P., Yamazaki, T., Geldmacher, J., Gee, J.S., Pressling, N., Hoshi, H., Anderson, L., Beier, C., Buchs, D.M., Chen, L.H., Cohen, B.E., Deschamps, M., Dorais, J., Ebuna, D., Ehmann, S., Fitton, J.G., Fulton, P.M., Ganbat, E., Hamelin, C., Hanyu, T., Kalnins, L., Kell, J., Machida, S., Mahoney, J.J., Moriya, K., Nichols, A.R.L., Rausch, S., Sano, S., Sylvan, J.B., and Williams, R., 2012. Limited latitudinal mantle plume motion for the Louisville Hotspot. Nature Geoscience, 5(12):911–917. https://doi.org/10.1038/ngeo1638
- Moore, T.C., Jr., Rabinowitz, P.D., Borella, P.E., Boersma, A., and Shackleton, N.J., 1984. Introduction and explanatory notes. In Moore, T.C., Jr., Rabinowitz, P. D., et al., Initial Reports of the Deep Sea Drilling Project. 74: Washington, DC (US Government Printing Office), 3–39. https://doi.org/10.2973/dsdp.proc.74.101.1984
- Morgan, W.J., 1971. Convection plumes in the lower mantle. Nature, 230(5288):42–43. https://doi.org/10.1038/230042a0
- Morgan, W.J., 1981. Hotspot tracks and the opening of the Atlantic and Indian Oceans. In Emiliani, C. (Ed.), The Sea. 7: New York (Wiley), 443–487. https://adsabs.harvard.edu/full/1981LPICo.457....1M
- Müller, R.D., Royer, J.-Y., and Lawver, L.A., 1993. Revised plate motions relative to the hotspots from combined Atlantic and Indian Ocean hotspot tracks. Geology, 21(3):275–278.
  - https://doi.org/10.1130/0091-7613(1993)021<0275:RPMRTT>2.3.CO;2
- O'Connor, J.M., and Duncan, R.A., 1990. Evolution of the Walvis Ridge-Rio Grande Rise hot spot system: implications for African and South American plate motions over plumes. Journal of Geophysical Research: Solid Earth, 95(B11):17475–17502. https://doi.org/10.1029/JB095iB11p17475
- O'Connor, J.M., and Jokat, W., 2015a. Tracking the Tristan-Gough mantle plume using discrete chains of intraplate volcanic centers buried in the Walvis Ridge. Geology, 43(8):715–718. https://doi.org/10.1130/G36767.1
- O'Connor, J.M., and Jokat, W., 2015b. Age distribution of ocean drill sites across the Central Walvis Ridge indicates plate boundary control of plume volcanism in the South Atlantic. Earth and Planetary Science Letters, 424:179–190. https://doi.org/10.1016/j.epsl.2015.05.021
- O'Connor, J.M., and le Roex, A.P., 1992. South Atlantic hot spot-plume systems: 1. Distribution of volcanism in time and space. Earth and Planetary Science Letters, 113(3):343–364. https://doi.org/10.1016/0012-821X(92)90138-L
- Rohde, J., Hoernle, K., Hauff, F., Werner, R., O'Connor, J., Class, C., Garbe-Schönberg, D., and Jokat, W., 2013. 70 Ma chemical zonation of the Tristan-Gough hotspot track. Geology, 41(3):335–338. https://doi.org/10.1130/G33790.1
- Ryan, W.B.F., Carbotte, S.M., Coplan, J.O., O'Hara, S., Melkonian, A., Arko, R., Weissel, R.A., Ferrini, V., Goodwillie, A., Nitsche, F., Bonczkowski, J., and Zemsky, R., 2009. Global multi-resolution topography synthesis. Geochemistry, Geophysics, Geosystems, 10(3):Q03014. https://doi.org/10.1029/2008GC002332
- Sager, W., Hoernle, K., Höfig, T.W., Avery, A.J., Bhutani, R., Buchs, D.M., Carvallo, C.A., Class, C., Dai, Y., Dalla Valle, G., Del Gaudio, A.V., Fielding, S., Gaastra, K.M., Han, S., Homrighausen, S., Kubota, Y., Li, C.-F., Nelson, W.R., Petrou, E., Potter, K.E., Pujatti, S., Scholpp, J., Shervais, J.W., Thoram, S., Tikoo-Schantz, S.M., Tshiningayamwe, M., Wang, X.-J., and Widdowson, M., 2023. Expedition 391 summary. In Sager, W., Hoernle, K., Höfig, T.W., Blum, P., and the Expedition 391 Scientists, Walvis Ridge Hotspot. Proceedings of the International Ocean Discovery Program, 391: College Station, TX (International Ocean Discovery Program). <a href="https://doi.org/10.14379/iodp.proc.391.101.2023">https://doi.org/10.14379/iodp.proc.391.101.2023</a>
- Sager, W.W., Thoram, S., Engfer, D.W., Koppers, A.A.P., and Class, C., 2021. Late Cretaceous Ridge reorganization, microplate formation, and the evolution of the Rio Grande Rise Walvis Ridge hot spot twins, South Atlantic Ocean. Geochemistry, Geophysics, Geosystems, 22(3):e2020GC009390. https://doi.org/10.1029/2020GC009390
- Steinberger, B., and Torsvik, T.H., 2008. Absolute plate motions and true polar wander in the absence of hotspot tracks. Nature, 452(7187):620–623. https://doi.org/10.1038/nature06824
- Tarduno, J., Bunge, H.-P., Sleep, N., and Hansen, U., 2009. The bent Hawaiian-Emperor hotspot track: inheriting the mantle wind. Science, 324(5923):50–53. https://doi.org/10.1126/science.1161256
- Tarduno, J.A., and Cottrell, R.D., 1997. Paleomagnetic evidence for motion of the Hawaiian hotspot during formation of the Emperor seamounts. Earth and Planetary Science Letters, 153(3–4):171–180. https://doi.org/10.1016/S0012-821X(97)00169-6

- Tarduno, J.A., Duncan, R.A., Scholl, D.W., Cottrell, R.D., Steinberger, B., Thordarson, T., Kerr, B.C., Neal, C.R., Frey, F.A., Torii, M., and Carvallo, C., 2003. The Emperor seamounts: southward motion of the Hawaiian hotspot plume in Earth's mantle. Science, 301(5636):1064–1069. https://doi.org/10.1126/science.1086442
- Torsvik, T.H., Müller, R.D., Van der Voo, R., Steinberger, B., and Gaina, C., 2008. Global plate motion frames: toward a unified model. Reviews of Geophysics, 46(3):RG3004. https://doi.org/10.1029/2007RG000227
- Torsvik, T.H., Steinberger, B., Gurnis, M., and Gaina, C., 2010. Plate tectonics and net lithosphere rotation over the past 150 My. Earth and Planetary Science Letters, 291(1–4):106–112. https://doi.org/10.1016/j.epsl.2009.12.055
- Tozer, B., Sandwell, D.T., Smith, W.H.F., Olson, C., Beale, J.R., and Wessel, P., 2019. Global bathymetry and topography at 15 arc sec: SRTM15+. Earth and Space Science, 6(10):1847–1864. https://doi.org/10.1029/2019EA000658
- Tsai, V.C., and Stevenson, D.J., 2007. Theoretical constraints on true polar wander. Journal of Geophysical Research: Solid Earth, 112(B5):B05415. https://doi.org/10.1029/2005JB003923
- Woodworth, D., and Gordon, R.G., 2018. Paleolatitude of the Hawaiian hot spot Since 48 Ma: evidence for a mid-Cenozoic true polar stillstand followed by late Cenozoic true polar wander coincident with Northern Hemisphere glaciation. Geophysical Research Letters, 45(21):11632–11640. https://doi.org/10.1029/2018GL080787
- Zheng, L., Gordon, R.G., and Woodworth, D., 2018. Pacific plate apparent polar wander, hot spot fixity, and true polar wander during the formation of the Hawaiian Island and Seamount Chain from an analysis of the skewness of magnetic anomaly 20r (44 Ma). Tectonics, 37(7):2094–2105. https://doi.org/10.1029/2017TC004897